RSC Advances

TOC

By push-pull strategy highly efficient and photostable naphtho-difuran derivatives were designed to get improved intrinsic electron mobility (1.13 $cm^2V^{-1}s^{-1}$).

Influence of push-pull configuration on the electro-optical and charge transport properties of novel naphtho-difuran derivatives: A DFT Study

Aijaz Rasool Chaudhry[a,b,∗], R. Ahmed[a,*], Ahmad Irfan[c], Shabbir Muhammad[b], Shaari A.[a], Abdullah G. Al-Sehemi[c,d,e]

[a] Department of Physics, Faculty of Science, Universiti Teknologi Malaysia, UTM Skudai, 81310 Johor, Malaysia.

[b] Department of Physics, Faculty of Science, King Khalid University, Abha 61413, P.O. Box 9004, Saudi Arabia.

[c] Department of Chemistry, Faculty of Science, King Khalid University, Abha 61413, P.O. Box 9004, Saudi Arabia.

[d] Unit of Science and Technology, Faculty of Science, King Khalid University, Abha 61413, P.O. Box 9004, Saudi Arabia.

[e] Center of Excellence for Advanced Materials Research, King Khalid University, Abha 61413, P.O. Box 9004, Saudi Arabia.

Abstract

We present a density functional theory (DFT) study pertaining to electro-optical and charge transport properties of two novel derivatives of naphtho [2,1-b:6,5-b′] difuran (DPNDF) as investigated based on push-pull configuration. Both molecular structures of the designed derivatives are optimized, in ground state (S_0) as well as excited state (S_1), using density functional theory (DFT) and time-dependent density functional theory (TD-DFT) respectively. Push-pull configuration effect is studied meticulously for different electro-optical properties including adiabatic/vertical electron affinity (EAa)/(EAv), adiabatic/vertical ionization potential (IPa)/(IPv) and hole/electron reorganization energies λ_h/λ_e, hole/electron transfer integrals (V_h/V_e), hole/electron mobility and photostability as well. From our study we observe smaller λ_e, improved V_e and higher electron mobility for compound **1** compared to the parent molecule. Our calculated value of the electron mobility for compound **1** (2.43 $cm^2V^{-1}s^{-1}$), revealing it an efficient electron transport material. Moreover influence of the push-pull on the electronic structure has also been investigated by calculating their total and partial density of states (DOS). Taking the advantage of strong push-pull configurations effect on other properties, the study of designed chemical systems is extended to their nonlinear optical (NLO) properties. Our designed novel derivatives (**1** & **2**) exhibit

---
∗   corresponding Authors, Tel.: +966 7 241 8240
e-mail addresses: aijaz_bwp27@hotmail.com (Aijaz Rasool Chaudhry)
rashidahmed@utm.my (R. Ahmed)

significantly larger amplitude values for first hyperpolarizability with β_{total} equal to 209.420×10^{-30} esu for compound **1** and 333.830×10^{-30} esu for compound **2,** respectively. It has been found that the first hyperpolarizability and HOMO-LUMO energy gap are in inverse relationship for compound 1 and 2.

Keywords: Push Pull Effect; Photophysical; Electronic properties; Transfer integrals; Mobility.

1. Introduction

Push-pull is an important strategy widely used in organic semiconductor materials (OSMs) to tune the photophysical properties[1-4]. More recently, push-pull strategy is good approach to enhance the electronic and charge transport properties[5-8]. Stronger push-pull affect represents a signification charge separation on molecular geometry and dipole moment[6]. A push-pull configuration is usually consists of an electron donating group (EDG), π conjugation bridge and an electron withdrawing group (EWG) which is expressed as EDGs-π-EWGs. Such type of push-pull configuration with strong EDGs and EWG results in lowering the HOMO-LUMO energy gap E_g which leads to efficient intramolecular charge transfer[9] and material performance that is beneficial for designing excellent OSMs. OSMs with push-pull configuration[10-12] are immensely studied at both levels (theoretically and experimentally) due to light weight, low fabrication cost on flexible substrates and large area bendy displays. These advantages of OSMs give edge them over the silicon-based traditional inorganic semiconductors and have been attracted massive interest of academic researchers as well as their industrial partners because of their potential applications in photonics and electronic devices, such as organic field effect transistors (OFETs)[13-15], organic light emitting diodes (OLEDs)[16, 17], organic photo-voltaic (OPVs)[17, 18] and organic light emitting transistors (OLETs)[19].

OFETs are fabricated and produced by adding electron system with π-conjugation20, or aromatic compound21 which help in the orbital wave functions delocalization22 and establish a good relationship between the geometric and electronic structure23-28. Several experimental and theoretical research reports are available on thiophene containing materials for use in OFETs and OLEDs29-38. Push–pull effect on the

electronic, optical and charge transport properties of the benzo[2,3-b]thiophene derivatives has been studies theoritically[6]. However in the literature, only a very small number of investigations had been reported about the furan containing OFETs and OLEDs materials in the past[39-42]. Currently a considerable attention is being given to furan as basic building block for organic π-conjugated materials that are more stable and have given sign for their potential applications especially in OFETs and OLEDs[19, 43-48]. Binaphtha-furanyl has been reported as organic light-emitting transistors (OLETs)[19]. Recently diphenyl-naphtho [2,1-b:6,5-b′] difuran (DPNDF) has been experimentally synthesized and reported as a good hole transport OSMs for OFETs[49]. In our previous study[50], it has been also found that; furan ring is one of the best electron transport material because of demonstrating very low reorganization energy for electron λ (e).

No study on DPNDF with Push-pull strategy has been found in the literature so far. In our present work as a starting point the experimental crystal of DPNDF[49] has been used as parent molecule and two new structures were derived by employing push-pull approach where EDGs is attached on one side of the naphtho-difuran (NDF) ring and EWGs on other side (EDGs-π-EWGs). In these structures three CH_3/OCH_3 groups were attached as EDGs at position X, whereas three CN groups were attached as EWGs at position Y for structure **1/2**, respectively, (named Compound **1** and Compound **2**) in the text (see Scheme 1 and **Figure S1** of supporting information).

Compound 1; X=CH_3;   Y=CN

Compound 2; X=OCH_3;   Y=CN
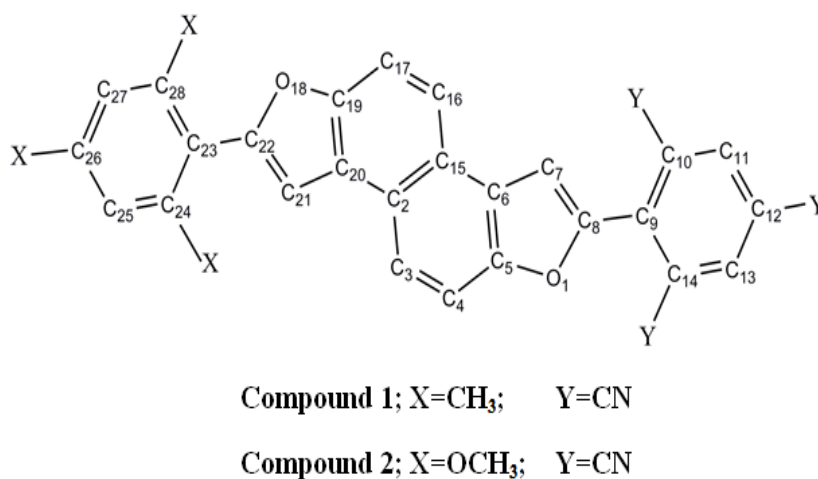
Scheme 1: Labeled diagram of DPNDF with position of attached groups

Derived geometries have been optimized in ground state (S_0) and first excited states (S_1) at the level DFT and TD-DFT respectively. Also the other properties such as highest occupied molecular orbitals (HOMOs), lowest unoccupied molecular orbitals (LUMOs), HOMO-LUMO energy gaps (E_g), adiabatic and vertical electron affinities (EAa/v), reorganization energies for hole λ (h)/electron λ (e), adiabatic and vertical ionization potentials (IPa/v), total/partial density of states (TDOS/PDOS), nonlinear optical properties (NLO), hole extraction potential (HEP), electron extraction potential (EEP), electronegativity (χ) are computed and discussed in detail. In addition the transfer integrals, mobility and photostability of these compounds have been evaluated. Moreover, push-pull effect is investigated on the above mentioned properties. A comparison of our obtained results is also made with experimental data where available.

2. Computational Methodology

DFT has been used to optimize the initial molecular structures for S_0 by applying the hybrid exchange correlation functional B3LYP[51-53] with 6-31G** basis sets[30, 39-42, 54-56]. For S_1 TD-DFT[56-59], via hybrid functional TD-B3LYP[60-63] with same basis set was used to optimize the geometries of the analogues. Electronic, photophysical properties including absorption (λa), and emission (λe) wavelengths have been calculated at the same level of theory. Reorganization energy (λ) represents the geometric relaxation energy of a molecule from charged (cation/anion) to the neutral state and from neutral to the charged (cation/anion) state (for detail see computational method expressed in supporting information). The reorganization energy for hole (λh) and electron (λe) was evaluated as:

$$\lambda_h = \lambda_+ + \lambda_1 \quad \text{and} \quad \lambda_e = \lambda_- + \lambda_2 \tag{1}$$

where the energy of geometry relaxation from neutral to charged (cation/anion) state is $\lambda_{+/-}$, and the relaxation energy of a molecule from charged (cation/anion) state to neutral is $\lambda_{1/2}$[64, 65]. These two terms are calculated directly from the adiabatic potential energy surfaces for $\lambda_{h/e}$[1, 66, 67]. In the next step, the calculations related to term transfer integrals are performed. To calculate the transfer integrals, inter-molecular nearest-neighboring hopping pathways have been generated using the single-crystal structure.

There are two widely employed approaches to obtain transfer integrals; one is Koopmans' theorem based method[68] and other one is direct evaluation method for the frontier molecular orbitals (FMOs)[69, 70]. We have used the direct approach[69, 70] to investigate the charge transport properties in this study. The hole/electron transfer integrals in this approach can be expressed as:

$$t_{h/e} = \left\langle \phi^{0,site1}_{LUMO/HOMO} \left| F^0 \right| \phi^{0,site2}_{LUMO/HOMO} \right\rangle \qquad (2)$$

here $t_{h/e}$ is the hole/electron transfer integrals, whereas $\phi^{0,site1}_{LUMO/HOMO}$ and $\phi^{0,site2}_{LUMO/HOMO}$ correspond to the HOMOs and LUMOs of the two consecutive molecules when there is no contact between the adjacent molecules, whereas F^0 is the Fock operator with unperturbed molecular orbitals for the dimer of a fixed pathway.

The carrier mobility μ can be evaluated with the help of Einstein relation as:

$$\mu = eD/k_BT \qquad (3)$$

here μ corresponds to the carrier mobility, D represents charge diffusion constant, e is for electronic charge, T is temperature and k_B donates the Boltzmann constant. Further detail related to transfer integrals and mobility can be seen in computational method expressed in supporting information. All these first-principles calculations were carried out using Gaussian 09 package[71].

For investigation of NLO response, we have calculated the static first hyperpolarizability (β_{tot}) and its components by finite field (FF) method. The FF method was broadly applied to investigate NLO because this methodology can be used in concert with the electronic structure method to compute β values[72-81]. In some very recent reports, β_{tot} calculated by this method is found to be substantiated with experimental structure property relationship[10, 82]. In FF method, a molecule is subjected to a static electric field (*F*), the energy (*E*) of the molecule is expressed by Eq. 2

$$E = E^{(0)} - \mu_1 F_1 - \frac{1}{2}\alpha_{ij}F_iF_j - \frac{1}{6}\beta_{ijk}F_iF_jF_k - \frac{1}{24}\gamma_{ijkl}F_iF_jF_kF_l - \cdots \qquad (4)$$

Where $E(0)$ is the energy of molecule in the absence of an electronic field, μ is the component of the dipole moment vector, α is the linear polarizability tensor, β and γ are the first and second hyperpolarizability tensors respectively, while i, j and k label the x, y and z components respectively. It is clear from Eq.4 that the values of μ, α, β, and γ can be obtained by differentiating E with respect to F. In our present investigation, we have calculated the molecular first hyperpolarizability. For a molecule, the components of the first hyperpolarizability can be calculated using the following Eq:

$$\beta_i = \beta_{iii} + \sum_{i \neq j} \left[\frac{(\beta_{ijj} + 2\beta_{jii})}{3} \right] \tag{5}$$

Using the x, y, z components, and the magnitude of first hyperpolarizability (β_{tot}) can be calculated by following Eq.

$$\beta_{tot} = \sqrt{(\beta_x^2 + \beta_y^2 + \beta_z^2)} \tag{6}$$

Where

$\beta_x = (\beta_{xxx} + \beta_{xxy} + \beta_{xyy})$,

$\beta_y = (\beta_{yyy} + \beta_{xxz} + \beta_{yyz})$,

$\beta_z = (\beta_{xzz} + \beta_{yzz} + \beta_{zzz})$

Therefore, the complete equation for calculating the magnitude of the total first static hyperpolarizability from GAUSSIAN 09 outputs is given by

$$\beta_{tot} = \left[(\beta_{xxx} + \beta_{xxy} + \beta_{xyy})^2 + (\beta_{yyy} + \beta_{xxz} + \beta_{yyz})^2 + (\beta_{xzz} + \beta_{yzz} + \beta_{zzz})^2 \right]^{1/2} \tag{7}$$

Since these β_{tot} values of GAUSSIAN 09 output files are reported in atomic units (a.u.), the calculated β_{tot} values were converted into electrostatic units (esu) (1 a.u. = 8.6393 x 10^{-33} esu). First hyperpolarizability is a third rank tensor that can be described by a $3 \times 3 \times 3$ matrix. The 27 components of the 3D matrix can be reduced to 10 components due to the Kleinman symmetry ($\beta_{xyy} = \beta_{yxy} = \beta_{yyx}$, $\beta_{yyz} = \beta_{yzy} = \beta_{zyy}$,... likewise other permutations also take same value).

3. Results and discussion

3.1. Ground and excited state geometries

The optimized values of bond lengths and bond/dihedral angles for the neutral, cation and anion structures have been tabulated in Table S1 of supporting information. For compound **1/2** the cation and anion structures differ from the neutral one. For compound **1**, alteration in the bond lengths C_{19}-C_{20}, C_{20}-C_{21}, C_{21}-C_{22}, C_{22}-C_{23}, C_{23}-C_{24} and C_{23}-C_{28} have been found; for cation as 0.021 Å, -0.032 Å, 0.37 Å, -0.033 Å, 0.026 Å and 0.023 Å; for anion as -0.003 Å, 0.00 Å, 0.001 Å, -0.001 Å, 0.004 Å and 0.002 Å, respectively; the bond angles C_{10}-C_9-C_{14}, O_{18}-C_{22}-C_{21} and O_{18}-C_{22}-C_{23} have been altered as 1.02°, -1.08° and 1.14° for cation whereas -1.86°, -0.24° and -0.04° for anion, respectively. Similarly the distortion in the dihedral angles C_{20}-C_{21}-C_{22}-C_{23}, O_{18}-C_{22}-C_{23}-C_{24}, O_{18}-C_{22}-C_{23}-C_{28}, C_{21}-C_{22}-C_{23}-C_{24} and C_{21}-C_{22}-C_{23}-C_{28} was found as -1.13°, 23.23°, -23.53°, -22.09° and 22.40° for cation; -0.69°, 4.25°, -4.34°, -3.64° and 3.74° for anion, respectively, as compared to their neutrals ones. The graphical representation bond lengths in Angstrom (Å) for compound 1 (left) and compound 2 (right) have been shown in Fig. 1 (a), respectively, for more clear understanding of the bond lengths alteration. The optimized coordinates of neutral, cation and anion structures for both the compounds have been tabulated in the Table S3, S4 and S5, respectively, in the supporting information.
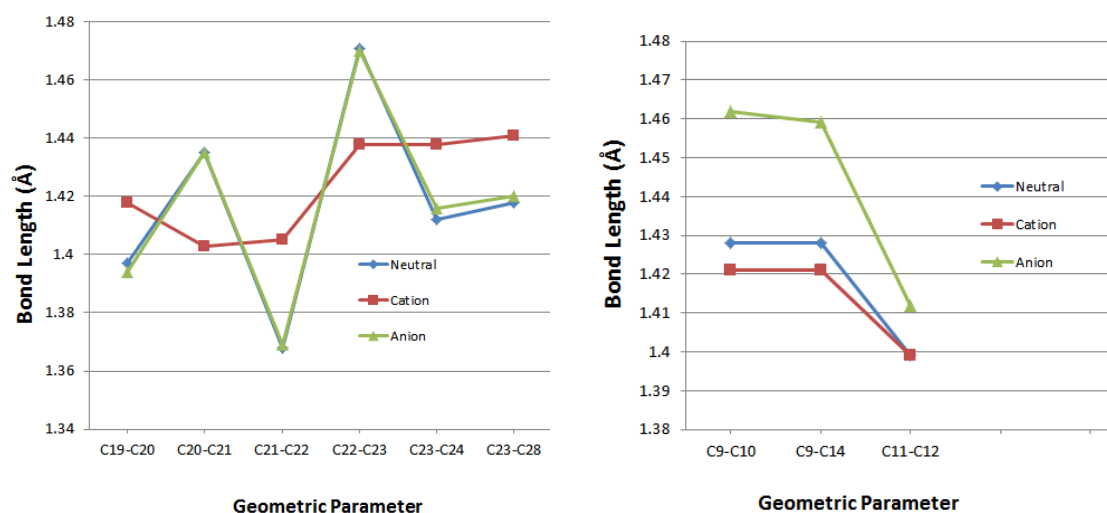
Fig 1(a): Selected optimized bond lengths in Angstrom (Å) for compound 1 (left) and compound 2 (right) of ground state (neutral, cation and anion) optimized at B3LYP/6-31G** level of theory.

For compound **2**, the bond lengths C_9-C_{10}, C_9-C_{14} and C_{11}-C_{12}, have been varied; for cation as -0.007, -0.007 and 0.00 Å; for anion as -0.034, 0.031 and 0.013 Å, respectively; the bond angles O_1-C_8-C_7, C_8-C_9-C_{14}, C_{10}-C_9-C_{14}, C_{10}-C_{11}-C_{12}, C_{11}-C_{12}-C_{13} and C_{12}-C_{13}-C_{14} have been altered as 0.67, -0.34, 1.02, -0.37, 0.58 and -0.47° for cation whereas as -1.19, 1.08, -1.83, 1.32, -1.50 and 1.09° for anion, respectively; similarly the distortion in the dihedral angles C_5-C_1-C_8-C_9, C_6-C_7-C_8-C_9, C_1-C_8-C_9-C_{10}, C_1-C_8-C_9-C_{14}, C_7-C_8-C_9-C_{10} and C_7-C_8-C_9-C_{14} was found as 0.37, 0.66, -10.12, 10.12, 9.39 and -9.40° for cation; 1.33, 1.65, 17.01, -16.75, -18.69 and 18.43° for anion, respectively, as compared to their neutrals ones.

The bond/dihedral angles (degree) have been represented graphical for compound 1 (left) and compound 2 (right) in Fig. 1 (b), respectively, for more clear understanding of the bond/dihedral angles distortion .The relaxation in geometric parameters of compound **1** cation structure was found more than the anion, whereas for compound **2**, the anion has more distortion as compared to the cation. This high distortion especially in bond/dihedral angles[83] might increase the reorganization energy of the compounds due to the more polarization caused by this distortion. Generally, it was stated that more relaxation in geometric parameters from neutral to anion/cation can increases the reorganization energy[2, 83].
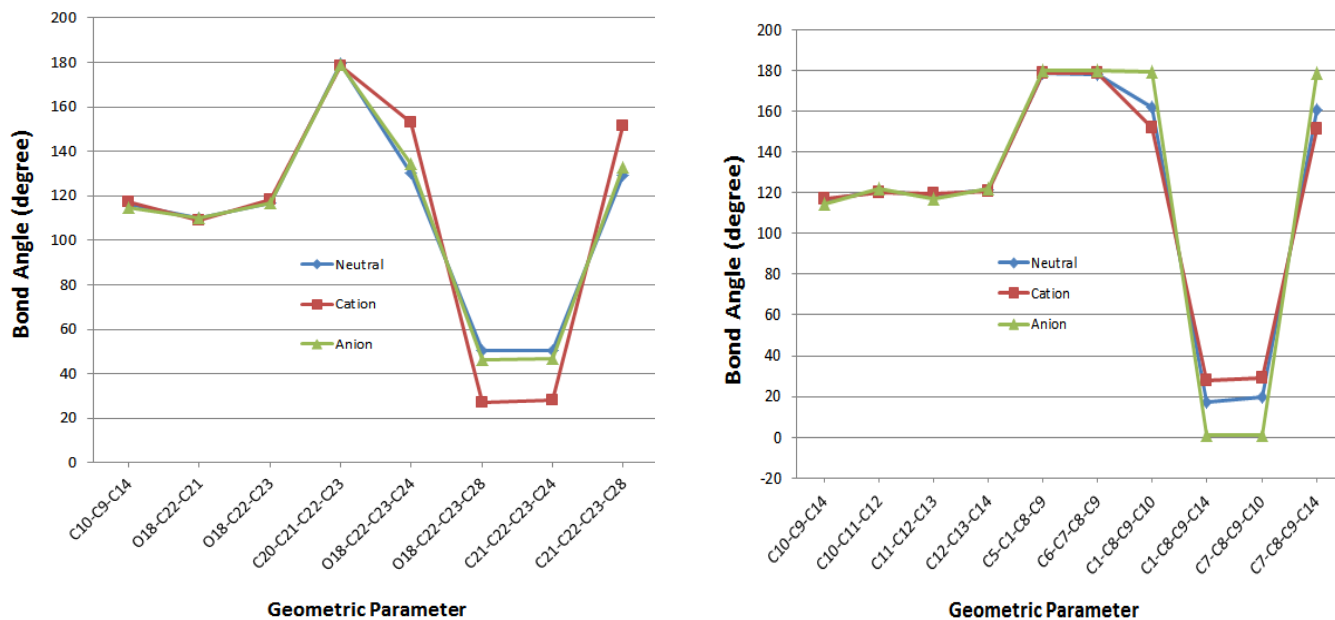
Fig 1(b): Selected optimized bond angles (degree) for compound 1 (left) and compound 2 (right) of ground state (neutral, cation and anion) optimized at B3LYP/6-31G** level of theory.

3.2. Electronic properties

3.2.1 Frontier molecular orbitals (ground and excited states)

HOMOs and LUMOs formation patterns for both the compounds at S_0 and S_1 have been formed at isosurfaces values of 0.02 and presented in Figure 2 (a) and 2(b), respectively. In compound **1**, for HOMO formation, it has been found that the charge is delocalized on C_7-C_8, C_5-C_6, C_3-C_4, C_2-C_{20}-C_{19}, C_{16}-C_{17}, C_{21}-C_{22}, C_{23}-C_{24} and C_{25}-C_{26} while on C_{10}, C_{12} and C_{14} charge is localized (lone-pair). Both the O atoms are not taking part in the formation of HOMO, whereas lone-pair has been formed on all N atoms. For LUMO formation the delocalization of charge has been found on C_2-C_3, C_5-C_6-C_{15}, C_7-C_8, C_8-C_9, C_{10}-C_{11}, and C_{13}-C_{14}. The charge is localized (lone-pair) on C_{17}, C_{20} and on all N atoms. Similar patterns of HOMO and LUMO formation have been found for compound **2** at S_0. Charge delocalization and localization behavior is following the same trend for compound **1/2** at S_1. It is clear from Fig. 2(a) that in the formation of HOMOs all the charge density has been distributed on EDGs and central core; for LUMOs the charge density has been shifted on EWGs revealing good intramolecular charge transfer for both the compounds.

Compound 1

Compound 2

HOMOs   LUMOs
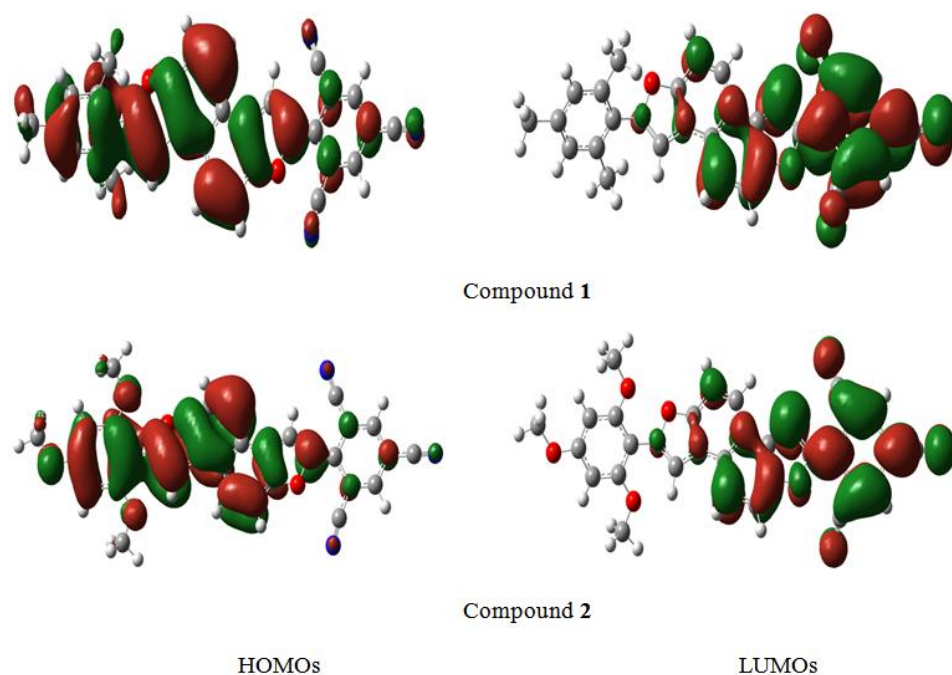
Fig 2(a): HOMOs and LUMOs formation patterns at ground state.

Compound **1**

Compound **2**

HOMOs   LUMOs
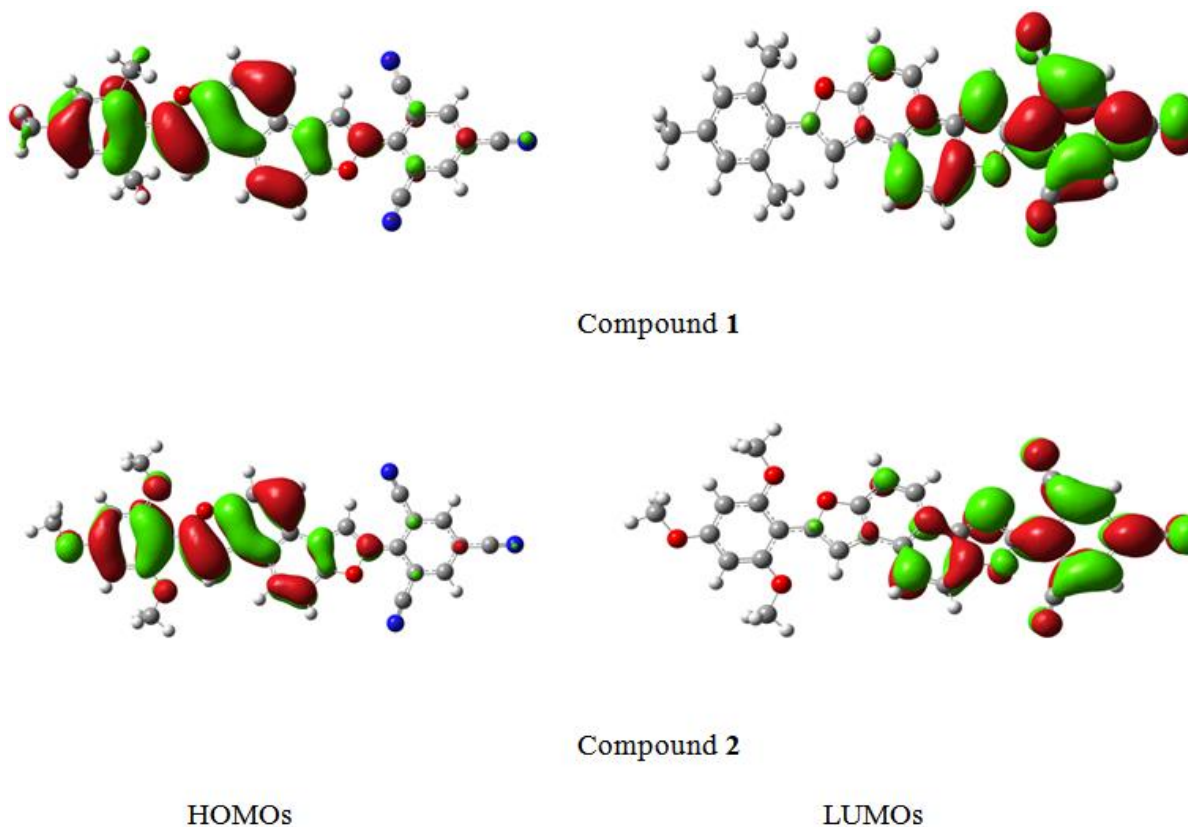
Fig 2(b): HOMOs and LUMOs spreading patterns at excited state.

The HOMO energies (E_{HOMO}), LUMO energies (E_{LUMO}) and HOMO-LUMO energy gaps (Eg) at S_0 and S_1 (in the brackets) states for both the compounds have been tabulated in Table 1. The graphical representation of E_{HOMO} and E_{LUMO} for S_0 / S_1 have been shown in Fig. 3 (left)/(right), respectively for more clear understanding of the E_g. E_{HOMO} of the compound **1** and **2** are -5.65 eV and -5.18 eV, respectively and in a good agreement with the experimental E_{HOMO} (-5.48 eV)[49] and computational E_{HOMO} (-5.10 eV)[84] of Parent molecule DPNDF. The trend of E_{HOMO} and E_{LUMO} are compound **1**(-5.65 eV, -2.93 eV) > compound **2** (-5.18 eV,-2.78 eV), respectively. Similar trend of E_{HOMO} and E_{LUMO} has been found at S_1 for both the compounds.

TABLE 1:

The $E_{HOMO}^{a,b}$, E_{LUMO} and E_g for S_0/S_1 states (in the brackets) at the B3LYP/6-31G** and TD-B3LYP/6-31G** levels of theory

Molecule	E_{HOMO}	E_{LUMO}	E_g
Compound **1**	-5.65	-2.93	2.72
	(-5.38)	(-3.05)	(2.33)
Compound **2**	-5.18	-2.78	2.40
	(-4.86)	(-2.86)	(2.00)

^{a}: Experimental data (E_{HOMO} = -5.48 eV) from ref [49]
^{b}: Computed values (E_{HOMO} = -5.10 eV) from ref [84]
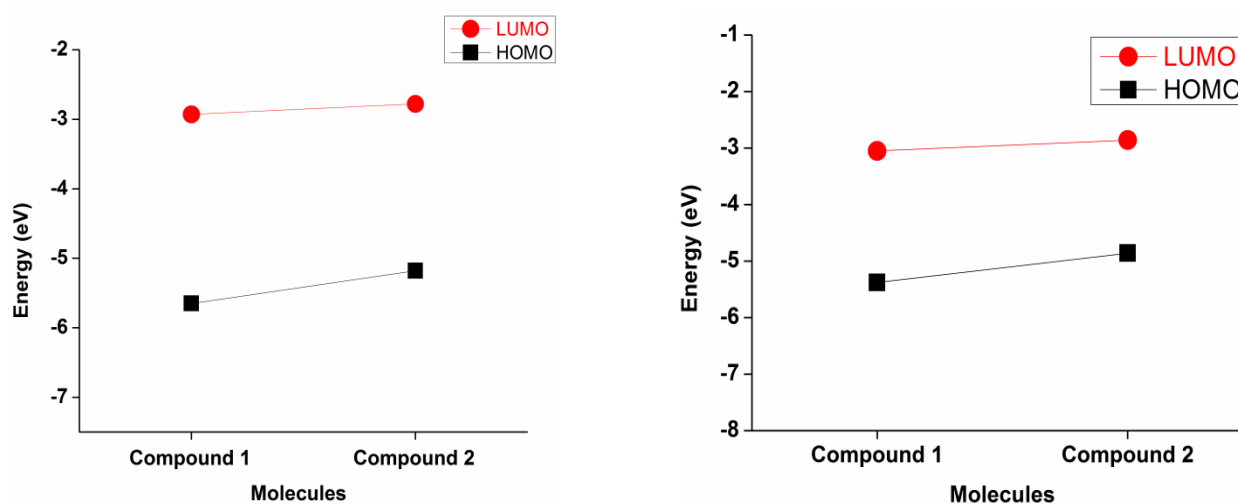
Fig 3: Comparison of E_{HOMO} and E_{LUMO} for ground (S_0) state (left)/excited (S_1) state (right) at the B3LYP/6-31G** and TD-B3LYP/6-31G** levels of theory

The energy gap is theoretically expressed as the difference of the orbital energies between HOMO and LUMO whereas experimentally it is the lowest energy transition from the S_0 to the S_1 state, and termed as the band gap which can be attained by the absorption spectra. When electron promotion takes place from HOMO to LUMO, quantitatively E_g can be approximately same as the optical band gap[1, 85-87]. The trend in the E_g is as compound **1** (2.72 eV) > compound **2** (2.40 eV) for S_0 and for S_1 is compound **1** (2.33 eV) >

compound **2** (2.00 eV). The smaller E_g of compound 2 reveals the red shift in the absorption and emission wavelengths in comparison with compound 1. Similarly the lower E_g of compound 2 illuminates the high charge transfer interaction[9, 88] within the compound 2. The high amplitude of first hyperpolarizability (β) is also correlates[9, 88] with lower E_g of a compound. We anticipate that the compound2 might show larger first hyperpolarizability (β) as compared to compound 1. It has been reported earlier that an electronic system with a smaller E_g might be more reactive[83, 84] than with a larger E_g, so compound 2 may be more reactive than compound 1 revealing that later one would be more stable.

It is expected that compounds having low-lying LUMO energy level might be thermodynamically more stable and charge transfer could not be quenched by electron loss. Moreover, according to Koopmann's theorem the LUMO energy is directly proportional to the EA. The higher LUMO energy level is illuminating that the electron injection barrier would be small resulting in the improvement of charge injection ability. It can be seen from Table 1, that the value of E_{LUMO} is increased in compound **1**and **2** as compared to the computed value of E_{LUMO} (-2.17 eV)[84] for the parent molecule DPNDF, which would decrease the electron injection barrier resulting in the improvement of the electron injection. Therefore it is expected that new compounds might be better materials as electron transporters.

3.3. Photophysical properties

The calculated absorption (λ_{abs}) and emission wavelengths (λ_{emis}), oscillator strengths (f) and HOMO-LUMO (H→L) contribution have been evaluated and tabulated in Table 2. The λ_{abs} and λ_{emis} against f are represented graphically in Fig. 4 (a) and (b), respectively. Table 2 shows the maximum H→L contribution at the S_0, which is 99% from H→L for compounds **1**and **2**, respectively. Similarly the maximum contribution of H→L for S_1 is H→L (99%) and H→L (100%) for compounds **1** and **2**, respectively. The $\lambda_{abs}/\lambda_{emis}$ have the red shift of 131/180 nm for compound **1** while 207/294 nm for compound **2**, respectively, as compared to the parent molecule of DPNDF ($\lambda_{abs}/\lambda_{emis}$ 381 /427 nm) as evaluated computationally[84], whereas the compound **2** has a red shift of 76 /114 nm as compared to the compound **1** for $\lambda_{abs}/\lambda_{emis}$,

respectively. This might be due to the strong EDGs and EWGs attached to the compound **2**. Structure-property relationship revealed that by substituting the EDG$_S$ and EWGs, the λ_{abs} and the λ_{emis} have shown red shifted behavior. The compound **1** may be orange while compound **2** would be red light emitters.

TABLE 2:

Calculated absorption (λ_{abs}), emission (λ_{emis}) wavelengths[a] (nm), oscillator strength (f) and HOMO-LUMO contribution for S$_0$ and S$_1$ States at the TD-DFT level of theories

Molecule	λ_{abs}	f	Contribution	λ_{emis}	f	Contribution
Compound **1**	512	0.467	H→L (99%)	607	0.373	H→L (99%)
Compound **2**	588	0.342	H →L (99%)	721	0.278	H→L (100%)

[a]: Computed values (λ_{abs}= 381 nm; λ_{emis}=427 nm) for comparison with ref. [84]

a   b
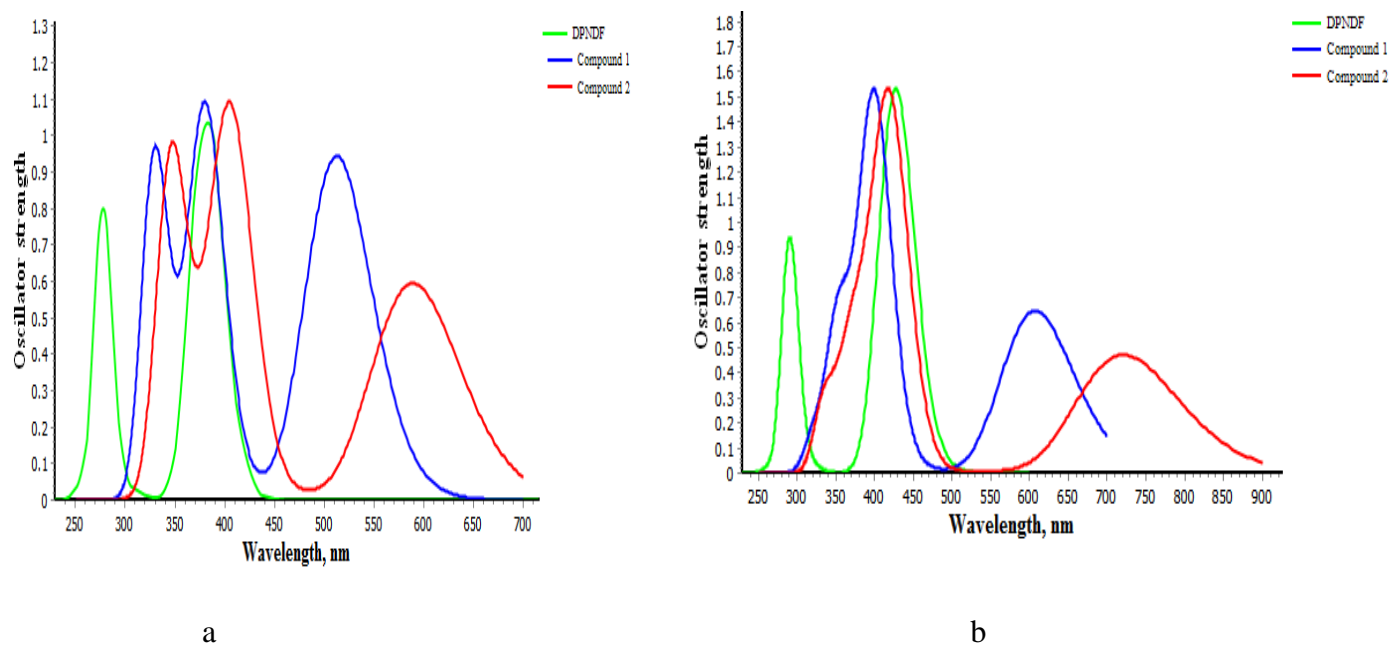
Fig 4 (a): Computed absorption spectra (b) computed emission spectra of compound **1** and **2** at TD-B3LYP/6-31G** levels of theory

3.4. Density of states

As the remarkable electro-optical properties are attributed to push-pull configuration in designed chemical systems, we have also calculated explicit contributions for the individual parts in the form of their PDOS shown in Fig. 5. We define three fragments for each compound; fragment one contains the phenyl ring with EWGs; fragment two is the central core (CC) and fragment three consists of the phenyl ring with EDGs. The individual fragment represents its contribution to the TDOS of the whole molecule as shown in the Fig. 5 with different curves. As shown in Fig. 5, for compound **1**, the peaks from -15.0 to -8.0 eV for the valance band; from 0.0 to 7.0 eV for conduction band are due to the similar contributions from EWGs, CC and EDG. At HOMO between -6.0 and -4.0 eV the major contribution is from CC, whereas EDG have minor contribution. On the other hand the EWG taking maximum part in conduction band (-3.0 and -2.0 eV) while CC has minimum contribution. Whereas EDG have no contribution in lower region of the conduction band while it has significant contribution between -1.0 to 0.0 eV and 2.0 to 7.0 eV. In TDOS the EDG contribution dominating in the lower valance bands from -13.0 to -9.0 eV and higher conduction bands 2.0 to 7.0 eV. The contribution of EDG is more in lower energy bonding molecular orbitals (-5.65 to -7.0 eV) while EWD contribution is larger in higher energy anti-bonding molecular orbitals (-2.93 to -3.5 eV), which facilitates as easy charge transfer during transition process of this push-pull configuration. This contribution of TDOS/PDOS from valance and conduction bands revealed good intramolecular charge transport from EDGs to EWGs. The high intramolecular charge transport from EDGs to EWGs leads to a very large value of β.Similar trend for TDOS and PDOS has been found in compound **2**.
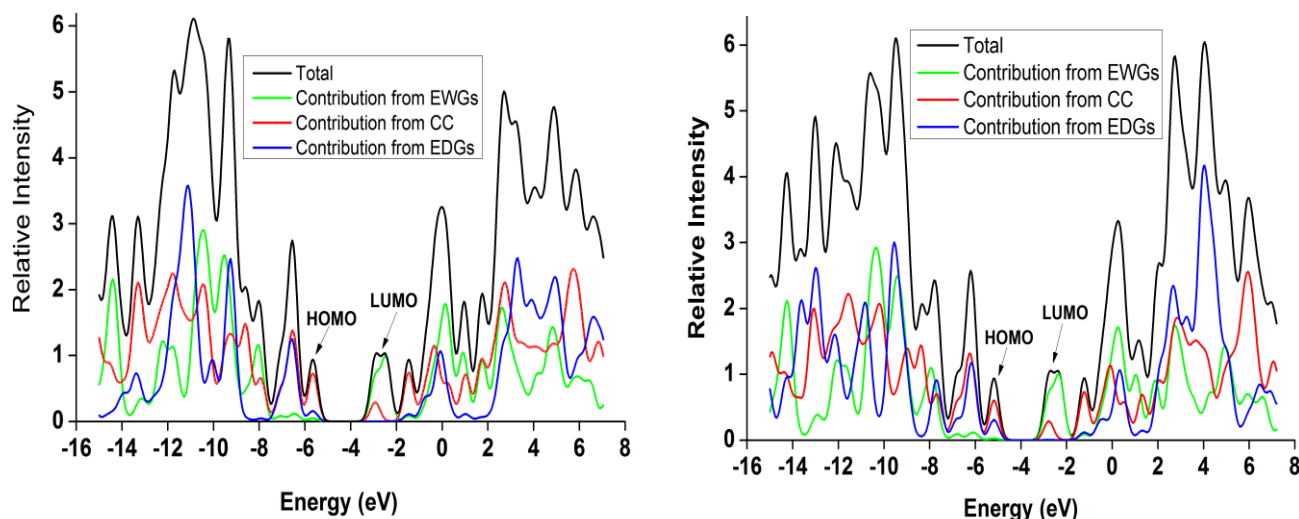
Fig 5: Graphical representation of TDOS and PDOS for compound **1**(left); compound **2** (right); computed at the B3LYP/6-31G** level of theory

3.5. Charge transfer properties

The EA and IP are the most essential properties to calculate the charge transport barriers, which were evaluated at the DFT/B3LYP/6-31G** level of theory. In OSMs lower IP and higher EA is very crucial to enhance the charge transport ability for electron and hole, respectively. The adiabatic/vertical IP (IPa/IPv) and adiabatic/vertical EA (EAa/EAv) of all derivatives have been calculated and tabulated in Table 3. A graphical comparison of the IPv, electronegativity and EAv has been drawn in Fig. 6 (left) to represent the results more clearly. In OFETs, the OMs having high EAv and small IPv might be better for n-type and p-type charge injection, respectively[89]. From Table 3, it is clear that compounds **1/2** have the EAv 1.63 /1.49 eV, respectively, which are higher than that of parent molecule DPNDF (0.29 eV)[84]. Thus it is expected that new designed compounds might be much better electron transport materials as compared to DPNDF. The EAv follow the same trend like E_{LUMO} for both the compounds as it has been observed that the molecule with high E_{LUMO} has the higher EAv. It can be seen from Tables 1 and 3 that **1** has the highest E_{LUMO} (-2.93 eV) among the two compounds hence has the highest EAv (1.63 eV).

The reorganization energy is the quantity which is very important for estimation of the ability to carry the charge in solid[90, 91]. The reorganization energy at B3LYP/6-31G** level of theory for electron

λ(e)/hole λ(h) have been given in Table 3. A graphical representation of hole λ(h) and λ(e) has been given in Fig. 6 (right) to represent the trend for further clarity. The calculated λ(h) of the DPNDF is 0.17 eV[84] at same level of theory and is in good agreement with already computed value[49]. From Table 3, it is clear that compound **1** / **2** have the λ(h) and λ(e) as 0.32 / 0.42 eV and 0.24/1.87 eV, respectively. For compound **1** λ(h) is higher than λ(e), whereas for compound **2** λ(h) is lower than λ(e) . The alteration and distortion in the bond/dihedral angles of cation is more than the anion for compound **1** resulting more polarization[2, 83] so λ(e) for compound **1** is less than λ(h). On the other hand for compound **2**, the bond/dihedral angles distortion in anion is higher than the cation; might be due to this the λ(e) of compound **2** is much higher than λ(h). From this trend it is predicted that **1** would be good as an electron-transport material; and **2** might be good as hole-transport material, respectively. The values λ(e) for **1** is smaller than diphenyl-naphtho-dithiophene 0.34 eV[92] and oligofuran 0.40 eV[93] revealed that new designed compound **1** might be more efficient as electron transport material as compared to the formers one.

The electronegativities (χ) of the two compounds have been given in Table 3. The electronegativity is the power of an atom in molecule to attract electron towards itself. The molecules with high electronegativities might be more efficient as electron transport materials because it can pull more electrons towards itself, resulting high electron charge transfer[57, 71-73, 94]. The trend of electronegativities in compound **1**> compound **2** revealed that the former might be better as electron transport materials as compared to the latter. The reorganization energies decreased with the increase in electronegativities of the compounds. It is the same trend as for E_{LUMO} and EAv of the two compounds.

TABLE 3:

The vertical/adiabatic Ionization potential and Electron affinity, hole extraction potential, electron extraction potential, electronegativity and the reorganization energy for hole[a] λ(h)/electron λ(e) at the B3LYP/6-31G** level of theory. All values in eV.

	Compound **1**	Compound **2**
IP (vertical)	6.85	6.37
IP (adiabatic)	6.68	6.15
HEP	6.53	5.95
EA (vertical)	1.63	1.49
EA (adiabatic)	1.76	1.61
EEP	1.87	3.36
χ	4.24	3.93
λ(h)	0.32	0.42
λ(e)	0.24	1.87

[a]: Data for comparison (λ(h) = 0.17 eV) from ref [49]
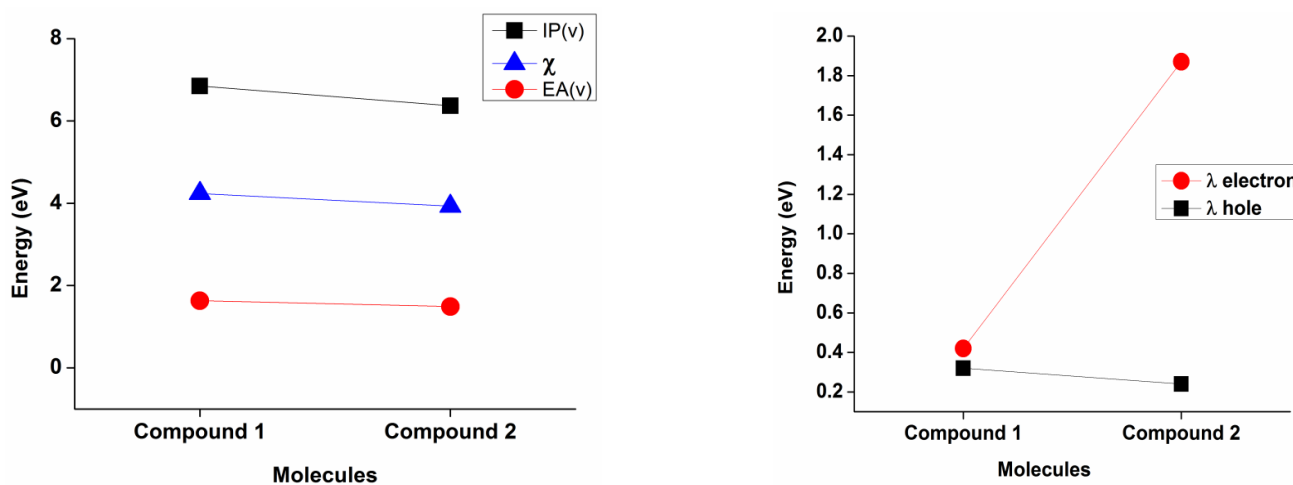
Fig 6: Graphical representation of IPv, Electronegativity and EAv (left); λ(h) and λ(e) (right) calculated at the B3LYP/6-31G** level of theory

3.5. First hyperpolarizability

It is well know that push-pull chemical configurations usually show remarkable NLO responses. In present investigation taking the advantage of strong push-pull configurations, we have also spotlighted the NLO responses of our designed chemical systems by calculating their static first hyperpolarizabilities. The calculated values of hyperpolarizability (β) along with their individual tensor components have been shown in Table 4. A well-established electronic communication of two different parts of a push-pull molecule is usually accompanying larger amplitude of its first hyperpolarizability which perhaps the case in our present designed compounds **1** and **2**. In Table 4, it can be seen that the calculated amplitudes of first hyperpolarizability (β_{tot}) for compound **1** and **2** are significantly larger with β_{tot} values of 209.420×10^{-30} esu and 333.830×10^{-30} esu., respectively. These values of first hyperpolarizability of compound **1** and **2** are much larger than that of proto-type urea molecule [β for urea is 0.3728×10^{-30} esu]. These total hyperpolarizability values are dominated by their diagonal components (components along dipole moment axis) of β_{xxx}. This is because there is significant charge transfer from EDGs to EWGs along x-axis. It can be seen from Table 1and Table 4 the first hyperpolarizability and E_g are in inverse relationship for both the compound, which support our prediction on basis of E_g Thus our designed systems have significant potential for NLO applications with good stability and large first hyperpolarizability amplitudes.
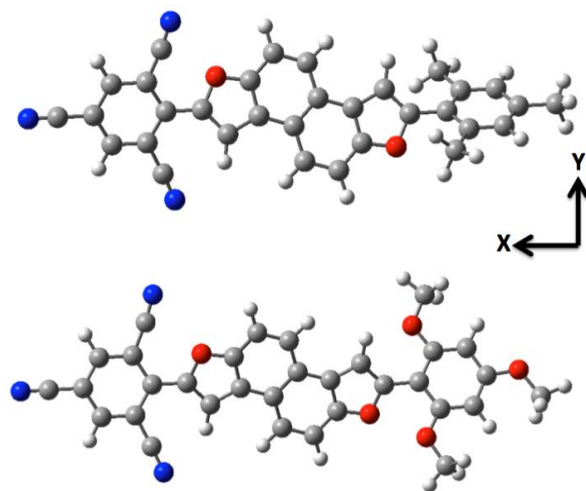
Fig 7: The definition of Cartesian axis for compound **1** and **2** optimized structures

Table 4:

The calculated values of polarizability (α) and hyperpolarizability (β) along their individual tensor components

Compound **1**			Compound **2**		
Components	a.u.	$(\times 10^{-30})$ esu	Component	a.u.	$(\times 10^{-30})$ esu
β_{xxx}	-24305	200.100	β_{xxx}	-38827	-335.500
β_{xxy}	-676	-5.841	β_{xxy}	-881	-7.613
β_{xyy}	-59	-0.509	β_{xyy}	119	1.028
β_{yyy}	7	0.0604	β_{yyy}	17	0.146
β_{xxz}	102	0.881	β_{xxz}	-362	-3.128
β_{xyz}	-90	-0.777	β_{xyz}	-103	-0.890
β_{yyz}	-30	-0.259	β_{yyz}	-8	-0.069
β_{xzz}	137	1.183	β_{xzz}	86	0.743
β_{yzz}	11	0.095	β_{yzz}	-3	-0.025
β_{zzz}	0	0.000	β_{zzz}	18	0.155
β_{tot}	**24236**	**209.420**	β_{tot}	**38633**	**333.830**

3.6. Molecular simulation

In our previous study [95], we have optimized the initial geometry of parent molecule at S_0 by hybrid functional B3LYP along with 6-31G** basis set using GAUSSIAN09 package. The crystal structure is simulated using facilities provided within Materials Studio (MS) package using the same lattice parameters as used for experimental crystal of DPNDF[49]. The crystal was simulated using Molecular Mechanics (MM) simulation approach, and the energy of the crystal was minimized by FORCITE module[96] with P21/c space group as available in MS package, considered to be a good tool for this purpose. DREIDING force field [97] has been used, which is suitable for these kinds of OMs with C, H, O, and N atoms. The simulated crystal structure was found in a nice agreement with the experimentally synthesized structure (see Fig.8). In that study we described the four pathways to compute the transfer integrals and mobility. Previously, main

computed transfer integral for parent molecule DPNDF was 36.9 meV[95] using Gaussian package at B3LYP/6-31 G** level and was closer to the available data of the same crystal 39.9 meV evaluated by ADF program[49]. Similarly the computed mobility was (1.1 cm^{2}V^{-1}s^{-1}) and shows a friendly agreement with experimentally measured value (1.30 cm^{2}V^{-1}s^{-1}). These results revealed that our adopted approach was reliable to build the crystal, compute the transfer integrals and mobility. In current study the same approach has been used to simulate the crystal structures for new designed compounds.
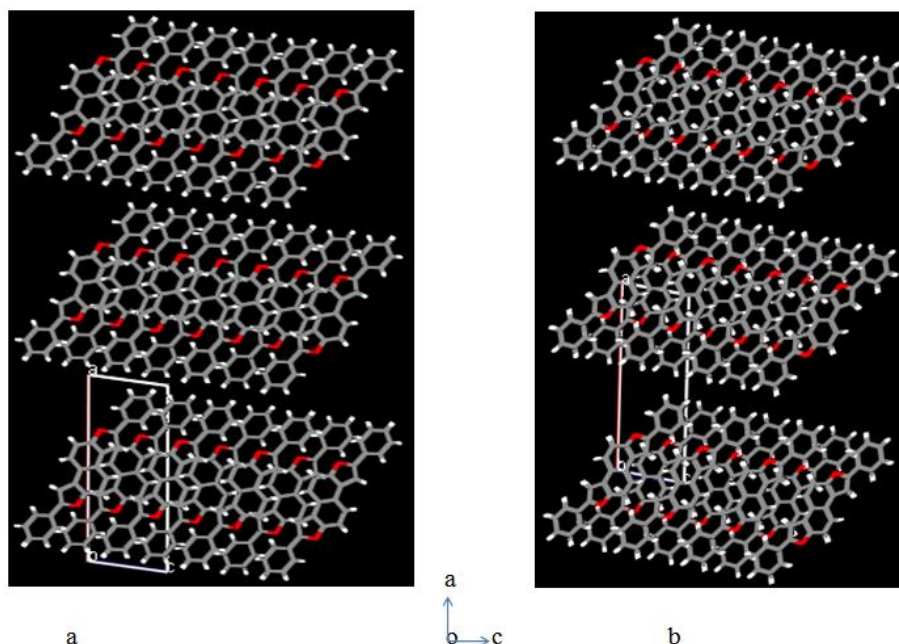
Fig 8: Experimental (a) and simulated (b) crystal structure of DPNDF along (aoc) direction.

3.7. Transfer integrals

We have also evaluated four discrete nearest neighboring hopping pathways for the two compounds. Transfer integrals for electron and hole have been evaluated using the method expressed in Equation 2 and presented in Table 5. A graphical comparison of hole and electron transfer integrals has been shown in Fig. 9 (a) (left) for more clear representation. It has been observed that some transfer integrals have negligibly small values so they are not discussed in text. The strongest hole /electron transfer integrals for **1** are 65.1 /118.4 meV and for **2** are 12.9 /-92 meV, respectively. It is clear from Table 5 that the compound **1** has the electron transfer integrals higher than that of compound **2**, revealing the compound **1** as better electron transport material as compared to the compound **2**.

TABLE 5:

The Transfer integrals (meV), Mass Centers (Å) and mobilities ($cm^2/V.s$) for hole and electron for DPNDF and its derivatives computed with DFT

Molecules	Pathways	Transfer Integrals[c]		Mass Centers	Mobility[c]	
		V_h[a]	V_e		Hole[b]	Electron
Compound **1**	i	65.1	114.1	5.071	0.49	2.09
	ii	-20.6	118.4	5.078	4.89×10^{-3}	2.43
	iii	-2.9	6.2	7.661	4.37×10^{-6}	4.15×10^{-5}
	iv	-15.9	5.7	19.106	2.46×10^{-2}	1.85×10^{-4}
Compound **2**	i	12.9	67	5.078	5.89×10^{-3}	2.66×10^{-8}
	ii	-6.5	-92	7.661	8.64×10^{-4}	2.15×10^{-7}
	iii	2.65×10^{-3}	6.64×10^{-3}	11.969	5.84×10^{-17}	1.43×10^{-23}
	iv	-0.15738	0.21216	19.108	1.85×10^{-9}	3.79×10^{-17}

[a]: V_h (39.9 meV) by other method from ref [49]

[b]: Experimental hole mobility (1.30 cm^2/V s) from ref.[49]

[c]: Computed values from ref.[95]
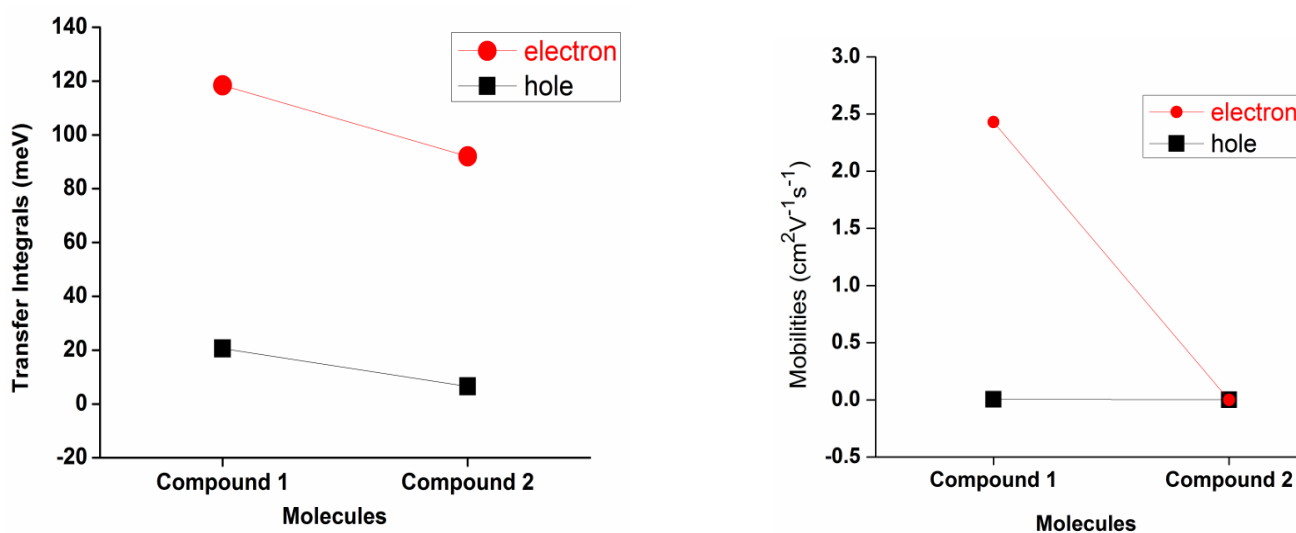
Fig 9 (a): Graphical representation hole/electron transfer integrals (left) and mobilities (right) computed with DFT

3.8. Mobility

Hole and electron mobilities of the both compounds for 4 pathways have been calculated and tabulated in Table 5. A graphical representation of hole and electron mobilities has been shown in Fig. 9 (a) (right) for more clear comparison. In our previous study[95] we have computed the mobility of the parent crystal DPNDF using the direct method and found the hole mobility as 1.1 $cm^2V^{-1}s^{-1}$, and in a nice agreement with the experimentally calculated mobility 1.30 $cm^2V^{-1}s^{-1}$ of the DPNDF[49]. Then we have used the same method for our current study for the four nearest neighboring molecules and found some of the pathways have the very low mobility for hole and electron; hence not discussed in the text, only highest hole/electron mobilities for two pathways of each compound have been discussed in detail. The hole mobilities of the two pathways have been found as $(0.49/4.89\times10^{-3})$ $cm^2V^{-1}s^{-1}$ and $(5.89\times10^{-3}/8.64\times10^{-4})$ $cm^2V^{-1}s^{-1}$ for compound **1** and **2**, whereas the electron mobilities of the two pathways are found as; $(2.09/2.43)$ $cm^2V^{-1}s^{-1}$, $(2.66\times10^{-8}/2.15\times10^{-7})$ $cm^2V^{-1}s^{-1}$ for compound **1** and **2**, respectively. It can be seen that the compound **1** exhibit highest electron mobility 2.43 $cm^2V^{-1}s^{-1}$ for specific 2nd pathway, which is higher than the already computed electron mobility 1.10 $cm^2V^{-1}s^{-1}$ of the parent molecule DPNDF.

The four pathways have been shown in the Fig. 9 (b) for more clear understanding of dimers packing which may affect the mobilities[30, 49]. These highest electron mobility values of 1st and 2nd pathways are in the stacking direction and might be due to smallest distance between the two molecules of the dimers. This packing and distance allowed maximum overlapping of the orbitals ensuing enhanced mobilities, whereas the 3rd and 4th pathways have side to side packing and greater distance between two molecules, which might be the reason for lowest mobilities.

The highest electron mobilities for compound **1** is several times higher than DPNDF[49] and α-Oligofuran[93] 0.0134 $cm^2V^{-1}s^-1$, hence predicted as good electron transport material in comparison with DPNDF and α-Oligofuran. It might be due to the attached EWGs (-CN), push-pull effect and comprehensible intra-molecular charge transfer from donor to acceptor moieties. From the highest average electron/hole intrinsic mobilities $(1.13/0.13)$ and $(6.08\times10^{-8}/1.69\times10^{-3})$ $cm^2V^{-1}s^{-1}$ for compound 1 and 2,

respectively, we anticipate that the compound **1** is good electron transport material; compound **2** may be hole transport material. These results support our prediction about the same materials in terms of E_{LUMO}, IP_v, EA_v and reorganization energies for hole and electron.
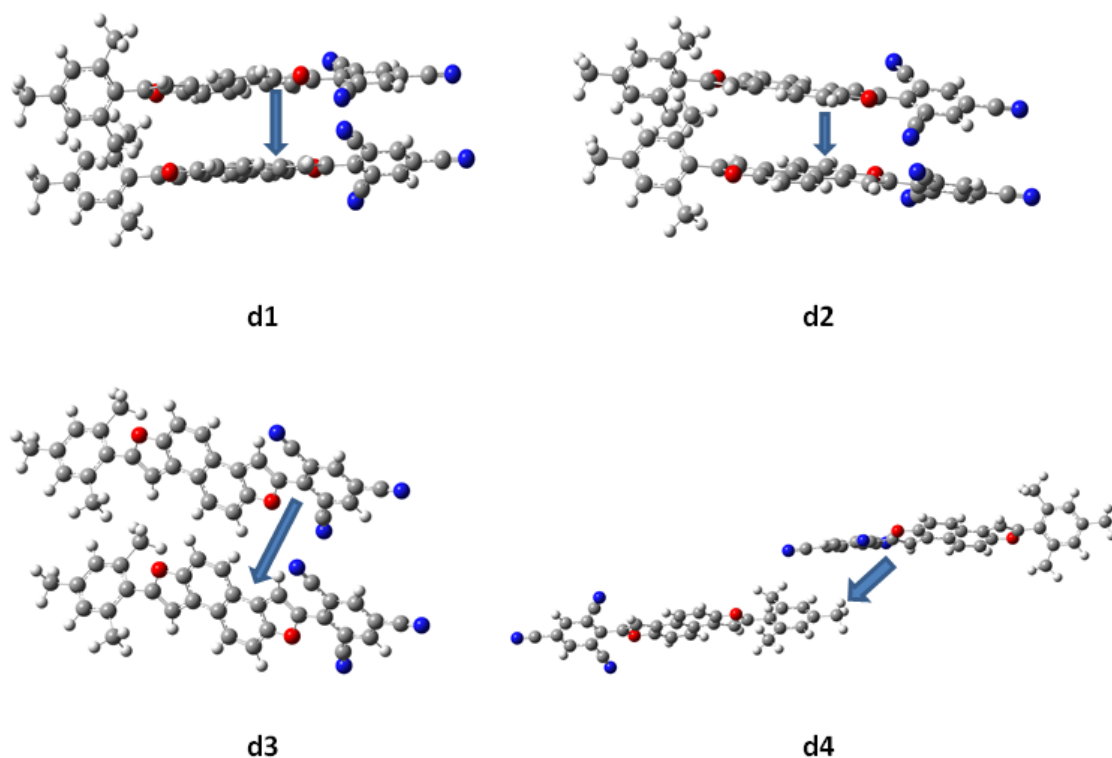
Fig 9 (b): The dimers investigated in present study to calculate the transfer integrals and mobilities.

3.9. Photostability

Molecular electrostatic surface potentials of all compounds have been mapped onto a total electron density surface as shown in Fig. 10. High electron density regions and low electron density regions are shown in indigo and green colors, respectively. High electron density is distributed on O and N atoms in studied systems. Previously, the photostability of organic materials was explained on the basis of molecular electrostatic surface potentials [56]. Recently, we pointed out that more electron density distributed on the system would favor to enhance the photostability[98]. In last study we observed that in the parent molecule DPNDF, the high electron density is distributed on oxygen atoms[95] (see Fig.S2 of supporting information). By substituting the EDGs and EWGs photostability augmented in designed molecules. The substitution of –

CH$_3$ and –CN at outer phenyl rings in **1** improve the photostability compared to Parent DPNDF molecule. High electron density distribution in **2** is covering more area due to the –OCH$_3$ and –CN than **1** revealing that former would be more photostable than that of later compound, that is due to strong EDGs (–OCH$_3$) attached with **2**. We noticed that by increasing the size and strength of EDGs photostability might be enhanced. Higher the electron density in **2** would decrease the oxidation resulting improve the photostability, which is in good agreement with our previous study[99].

Compound 1
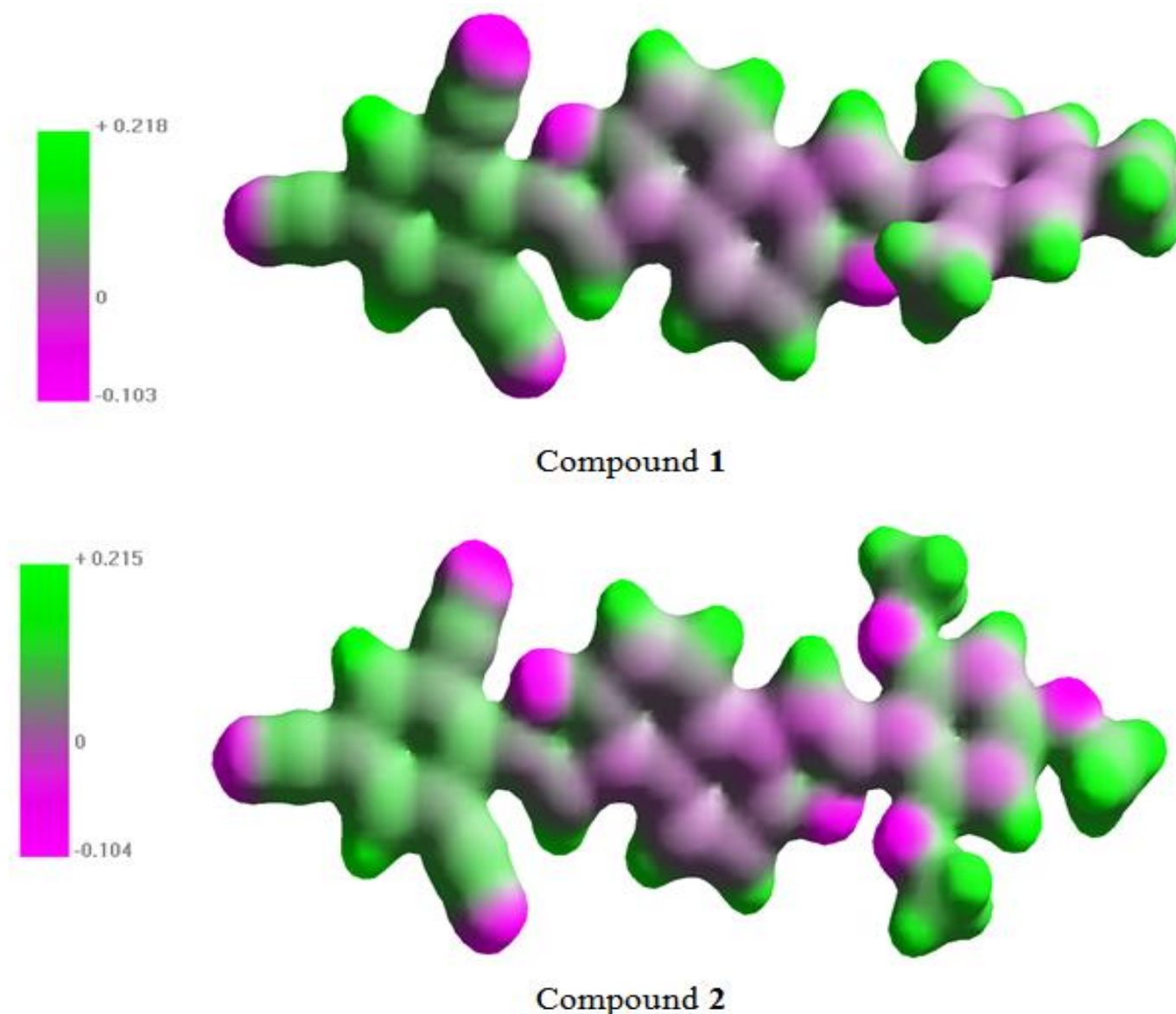
Compound 2

Fig 10: Molecular electrostatic potential surfaces of two compounds.

4. Conclusions

Thus the push-pull configurations have shown interesting effects to tune the electro-optical properties of compounds **1** and **2**. In the light of our present DFT investigation, we can draw following interesting conclusions:

1. The two designed novel compounds have the higher EAv values as compared to their parent molecule DPNDF.

2. The absorption and emission spectra of designed compounds **1** and **2** have shown the red shift as compared to their parent molecule. This is because of well-established communication between donor and acceptor parts. The HOMOs and LUMOs in both the studied compounds are delocalized as well as localized on central core and EWGs, respectively. The EWGs are taking part in the establishment of LUMOs only. The HOMO energies are in a nice agreement with the experimentally estimated HOMO of the parent molecule DPNDF.

3. The influence of the push-pull parts has been investigated by calculating their total and partial density of states (DOS).

4. Taking the advantage of strong push-pull configurations, our designed chemical systems have also been rationalized as efficient NLO materials with significantly larger amplitudes of first hyperpolarizability for compounds **1** and **2**.

5. The first hyperpolarizability and HOMO-LUMO energy gap are in inverse relationship for compound 1 and 2.

6. The electron transfer integrals and electron mobility have been enhanced significantly in compound **1** by introducing the -CH$_3$ and -CN groups, respectively. So it is predicted that the compound **1** would be a good electron transport material as compared to compound **2** and the parent molecule DPNDF.

7. The photostability has been enhanced significantly in compound **2** by introducing the -OCH$_3$ and -CN groups, because of enriched electron density distributed on these groups. As a result it is predicted that **2** would be more stable than **1.**

Hence, we expect that these compounds would serve as excellent candidates for OFET, OLET and OLED applications with enhanced photostability.

Acknowledgement

References

1.   Y. Li, L.-Y. Zou, A.-M. Ren and J.-K. Feng, *Comput. Theor. Chem.*, 2012, **981**, 14.
2.   A. Irfan, R. Cui, J. Zhang and L. Hao, *Chem. Phys.*, 2009, **364**, 39.
3.   A. É. Masunov and P. M. Zorkii, *J. Struct. Chem.*, 1992, **33**, 423.
4.   S. Ananthavel and M. Manoharan, *Chem. Phys.*, 2001, **269**, 49.
5.   A. Irfan, A. G. Al-Sehemi and S. Muhammad, *Synth. Met.*, 2014, **190**, 27.
6.   A. Irfan, A. G. Al-Sehemi and M. S. Al-Assiri, *Comput. Theor. Chem.*, 2014, **1031**, 76.
7.   A. Irfan, A. G. Al-Sehemi and M. S. Al-Assiri, *J. Fluorine Chem.*, 2014, **157**, 52.
8.   A. Irfan, A. G. Al-Sehemi and M. S. Al-Assiri, *J. Mol. Graphics Modell.*, 2013, **44**, 168.
9.   H. Alyar, *Rev. Adv. Mater. Sci.*, 2013, **34**, 79.
10.   P. Srinivasan, T. Kanagasekaran and R. Gopalakrishnan, *Crystal Growth & Design*, 2008, **8**, 2340.
11.   M. Rao, R. Ponce Ortiz, A. Facchetti, T. J. Marks and K. S. Narayan, *J. Phys. Chem. C*, 2010, **114**, 20609.
12.   I. Osaka, T. Abe, M. Shimawaki, T. Koganezawa and K. Takimiya, *ACS Macro Letters*, 2012, **1**, 437.
13.   H. E. Katz, *J. Mater. Chem.*, 1997, **7**, 369.
14.   G. Horowitz and M. E. Hajlaoui, *Adv. Mater.*, 2000, **12**, 1046.
15.   C. R. Newman, C. D. Frisbie, D. A. da Silva Filho, J.-L. Brédas, P. C. Ewbank and K. R. Mann, *Chem. Mater.*, 2004, **16**, 4436.
16.   C. W. Tang and S. A. VanSlyke, *Appl. Phys. Lett.*, 1987, **51**, 913.
17.   P. K. H. Ho, J.-S. Kim, J. H. Burroughes, H. Becker, S. F. Y. Li, T. M. Brown, F. Cacialli and R. H. Friend, *Nature*, 2000, **404**, 481.
18.   F. Padinger, R. S. Rittberger and N. S. Sariciftci, *Adv. Funct. Mater.*, 2003, **13**, 85.
19.   K. Niimi, H. Mori, E. Miyazaki, I. Osaka, H. Kakizoe, K. Takimiya and C. Adachi, *Chem. Commun.*, 2012, **48**, 5892.
20.   A. W. Hofmann, *Proc. R. Soc. Lond.*, 1856, **8**, 1.
21.   IUPAC, *Compendium of Chemical Terminology (the "Gold Book"), 2nd edn. Compiled by A. D. McNaught and A. Wilkinson*, 1997.
22.   P. v. R. Schleyer, *Chem. Rev.*, 2005, **105**, 3433.
23.   J.-L. Brédas, D. Beljonne, V. Coropceanu and J. Cornil, *Chem. Rev.*, 2004, **104**, 4971.

24.   J.-L. Brédas, J. Cornil, D. Beljonne, D. A. dos Santos and Z. Shuai, *Acc. Chem. Res.*, 1999, **32**, 267.

25.   J. Cornil, D. A. dos Santos, X. Crispin, R. Silbey and J. L. Brédas, *J. Am. Chem. Soc.*, 1998, **120**, 1289.

26.   J. L. Bredas and G. B. Street, *Acc. Chem. Res.*, 1985, **18**, 309.

27.   A. Warshel and M. Karplus, *J. Am. Chem. Soc.*, 1974, **96**, 5677.

28.   S.-C. Yang, W. Graupner, S. Guha, P. Puschnig, C. Martin, H. R. Chandrasekhar, M. Chandrasekhar, G. Leising, C. Ambrosch-Draxl and U. Scherf, *Phys. Rev. Lett.*, 2000, **85**, 2388.

29.   A. Irfan, M. Nadeem, M. Athar, F. Kanwal and J. Zhang, *Comput. Theor. Chem.*, 2011, **968**, 8.

30.   A. Irfan, A. G. Al-Sehemi, S. Muhammad and J. Zhang, *Aust. J. Chem.*, 2011, **64**, 1587.

31.   M. S. Wrackmeyer, M. Hein, A. Petrich, J. Meiss, M. Hummert, M. K. Riede and K. Leo, *Sol. Energy Mater. Sol. Cells*, 2011, **95**, 3171.

32.   S. Das, S. P. Senanayak, A. Bedi, K. S. Narayan and S. S. Zade, *Polymer*, 2011, **52**, 5780.

33.   J. A. Letizia, S. Cronin, R. P. Ortiz, A. Facchetti, M. A. Ratner and T. J. Marks, *Chem.--Eur. J.*, 2010, **16**, 1911.

34.   F. Buonocore and A. Matteo, *Theor. Chem. Acc.*, 2009, **124**, 217.

35.   Q.-X. Wu, Y. Geng, Y. Liao, X.-D. Tang, G.-C. Yang and Z.-M. Su, *Theor. Chem. Acc.*, 2012, **131**, 1.

36.   K. N. N. Unni, S. Dabos-Seignon and J.-M. Nunzi, *J. Mater. Sci.*, 2006, **41**, 317.

37.   P. Pingel, A. Zen, D. Neher, I. Lieberwirth, G. Wegner, S. Allard and U. Scherf, *Appl. Phys. A*, 2009, **95**, 67.

38.   H. Koezuka, A. Tsumura and T. Ando, *Synth. Met.*, 1987, **18**, 699.

39.   Y. Miyata, T. Nishinaga and K. Komatsu, *J. Org. Chem.*, 2005, **70**, 1147.

40.   Y. Miyata, M. Terayama, T. Minari, T. Nishinaga, T. Nemoto, S. Isoda and K. Komatsu, *Chem.--Asian J.*, 2007, **2**, 1492.

41.   O. Gidron, A. Dadvand, Y. Sheynin, M. Bendikov and D. F. Perepichka, *Chem. Commun.*, 2011, **47**, 1976.

42.   C.-C. Wu, W.-Y. Hung, T.-L. Liu, L.-Z. Zhang and T.-Y. Luh, *J. Appl. Phys.*, 2003, **93**, 5465.

43.   K. Kadac, M. J. Bosiak and J. Nowaczyk, *Synth. Met.*, 2012, **162**, 1981.

44.   M. Watanabe, W.-T. Su, Y. J. Chang, T.-H. Chao, Y.-S. Wen and T. J. Chow, *Chem.--Asian J.*, 2013, **8**, 60.

45.   M. Nakano, S. Shinamura, Y. Houchin, I. Osaka, E. Miyazaki and K. Takimiya, *Chem. Commun.*, 2012, **48**, 5671.

46.   M. Nakano, K. Niimi, E. Miyazaki, I. Osaka and K. Takimiya, *J. Org. Chem.*, 2012, **77**, 8099.

47.   K. Mitsudo, J. Harada, Y. Tanaka, H. Mandai, C. Nishioka, H. Tanaka, A. Wakamiya, Y. Murata and S. Suga, *J. Org. Chem.*, 2013, **78**, 2763.

48.   H. Chen, W. Delaunay, J. Li, Z. Wang, P.-A. Bouit, D. Tondelier, B. Geffroy, F. Mathey, Z. Duan, R. Réau and M. Hissler, *Org. Lett.*, 2013, **15**, 330.

49.   C. Mitsui, J. Soeda, K. Miwa, H. Tsuji, J. Takeya and E. Nakamura, *J. Am. Chem. Soc.*, 2012, **134**, 5448.

50.   A. R. Chaudhry, R. Ahmed, A. Irfan, A. Shaari and A. G. Al-Sehemi, *Mater. Chem. Phys.*, 2013, **138**, 468.

51.   P. J. Stephens, F. J. Devlin, C. F. Chabalowski and M. J. Frisch, *J. Phys. Chem.*, 1994, **98**, 11623.

52.   A. D. Becke, *J. Chem. Phys.*, 1993, **98**, 5648.

53.   C. Lee, W. Yang and R. G. Parr, *Phys. Rev. B*, 1988, **37**, 785.

54.   E. Cho, C. Risko, D. Kim, R. Gysel, N. Cates Miller, D. W. Breiby, M. D. McGehee, M. F. Toney, R. J. Kline and J.-L. Bredas, *J. Am. Chem. Soc.*, 2012, **134**, 6177.

55.   T. Sajoto, S. P. Tiwari, H. Li, C. Risko, S. Barlow, Q. Zhang, J.-Y. Cho, J.-L. Brédas, B. Kippelen and S. R. Marder, *Polymer*, 2012, **53**, 1072.

56.   A. Irfan, J. Zhang and Y. Chang, *Theor. Chem. Acc.*, 2010, **127**, 587.

57.   R. Bauernschmitt and R. Ahlrichs, *Chem. Phys. Lett.*, 1996, **256**, 454.

58.   C. Van Caillie and R. D. Amos, *Chem. Phys. Lett.*, 2000, **317**, 159.

59.   F. Furche and R. Ahlrichs, *J. Chem. Phys.*, 2002, **117**, 7433.

60.   G. Scalmani, M. J. Frisch, B. Mennucci, J. Tomasi, R. Cammi and V. Barone, *J. Chem. Phys.*, 2006, **124**, 094107.

61.   J. E. Lee, G. C. Choi, N. G. Park, Y. K. Ha and Y. S. Kim, *Curr. Appl. Phys.*, 2004, **4**, 675.

62.   M. C. Zwier, J. M. Shorb and B. P. Krueger, *J. Comput. Chem.*, 2007, **28**, 1572.

63.   E. Li, A. Kim and L. Zhang, *Comp Chem Moodle*, 2007, **1**, 01.

64.   N. E. Gruhn, D. A. da Silva Filho, T. G. Bill, M. Malagoli, V. Coropceanu, A. Kahn and J.-L. Brédas, *J. Am. Chem. Soc.*, 2002, **124**, 7918.

65.   J. R. Reimers, *J. Chem. Phys.*, 2001, **115**, 9103.

66.   A. Irfan, R. Cui and J. Zhang, *Theor. Chem. Acc.*, 2009, **122**, 275.
67.   V. Coropceanu, T. Nakano, N. E. Gruhn, O. Kwon, T. Yade, K.-i. Katsukawa and J.-L. Brédas, *J. Phys. Chem. B*, 2006, **110**, 9482.
68.   B. C. Lin, C. P. Cheng, Z.-Q. You and C.-P. Hsu, *J. Am. Chem. Soc.*, 2004, **127**, 66.
69.   A. Troisi and G. Orlandi, *Chem. Phys. Lett.*, 2001, **344**, 509.
70.   S. Yin, Y. Yi, Q. Li, G. Yu, Y. Liu and Z. Shuai, *J. Phys. Chem. A*, 2006, **110**, 7138.
71.   M. Frisch, G. Trucks, H. B. Schlegel, G. Scuseria, M. Robb, J. Cheeseman, G. Scalmani, V. Barone, B. Mennucci and G. Petersson, *Inc., Wallingford, CT*, 2009, **270**, 271.
72.   C. Dehu, F. Meyers and J. L. Bredas, *J. Am. Chem. Soc.*, 1993, **115**, 6198.
73.   S. Muhammad, M. R. S. A. Janjua and Z. Su, *J. Phys. Chem. C*, 2009, **113**, 12551.
74.   S. Muhammad, C. Liu, L. Zhao, S. Wu and Z. Su, *Theor. Chem. Acc.*, 2009, **122**, 77.
75.   S. Muhammad, H. Xu, Y. Liao, Y. Kan and Z. Su, *J. Am. Chem. Soc.*, 2009, **131**, 11833.
76.   H.-L. Xu, Z.-R. Li, Z.-M. Su, S. Muhammad, F. L. Gu and K. Harigaya, *J. Phys. Chem. C*, 2009, **113**, 15380.
77.   S. Muhammad, H. Xu, M. R. S. A. Janjua, Z. Su and M. Nadeem, *Phys. Chem. Chem. Phys.*, 2010, **12**, 4791.
78.   S. Muhammad, T. Minami, H. Fukui, K. Yoneda, R. Kishi, Y. Shigeta and M. Nakano, *J. Phys. Chem. A*, 2012, **116**, 1417.
79.   D. L. Wang, H. L. Xu, Z. M. Su, S. Muhammad and D. Y. Hou, *ChemPhysChem*, 2012, **13**, 1232.
80.   R.-L. Zhong, H.-L. Xu, S. Muhammad, J. Zhang and Z.-M. Su, *J. Mater. Chem.*, 2012, **22**, 2196.
81.   S. Muhammad, H. Xu, Z. Su, K. Fukuda, R. Kishi, Y. Shigeta and M. Nakano, *Dalton Transactions*, 2013, **42**, 15053.
82.   A. B. Ahmed, H. Feki, Y. Abid, H. Boughzala and A. Mlayah, *J. Mol. Struct.*, 2008, **888**, 180.
83.   Y. Xiaodi, L. Qikai and S. Zhigang, *Nanotechnology*, 2007, **18**, 424029.
84.   A. R. Chaudhry, R. Ahmed, A. Irfan, A. Shaari, H. Maarof and A. G. Al-Sehemi, *SAINS MALAYSIANA*, 2014, **43**, 867.
85.   P. J. Hay, *J. Phys. Chem. A*, 2002, **106**, 1634.
86.   A. Curioni, W. Andreoni, R. Treusch, F. J. Himpsel, E. Haskal, P. Seidler, C. Heske, S. Kakar, T. Van Buuren and L. J. Terminello, *Appl. Phys. Lett.*, 1998, **72**, 1575.
87.   S. Y. Hong, D. Y. Kim, C. Y. Kim and R. Hoffmann, *Macromolecules*, 2001, **34**, 6474.
88.   V. Arjunan, P. S. Balamourougane, C. V. Mythili and S. Mohan, *J. Mol. Struct.*, 2011, **1003**, 92.
89.   Y. Zhang, X. Cai, Y. Bian, X. Li and J. Jiang, *J. Phys. Chem. C*, 2008, **112**, 5148.
90.   R. A. Marcus, *Rev. Mod. Phys.*, 1993, **65**, 599.
91.   J. L. Brédas, J. P. Calbert, D. A. da Silva Filho and J. Cornil, *Proc. Natl. Acad. Sci.*, 2002, **99**, 5804.
92.   Y. Yi, L. Zhu and J.-L. Brédas, *J. Phys. Chem. C*, 2012, **116**, 5215.
93.   S. Mohakud, A. P. Alex and S. K. Pati, *J. Phys. Chem. C*, 2010, **114**, 20436.
94.   Y. Ie, Y. Umemoto, M. Okabe, T. Kusunoki, K.-i. Nakayama, Y.-J. Pu, J. Kido, H. Tada and Y. Aso, *Org. Lett.*, 2008, **10**, 833.
95.   A. R. Chaudhry, R. Ahmed, A. Irfan, A. Shaari and A. G. Al-Sehemi, *Sci. Adv. Mater.*, 2014, **6**, 1.
96.   W. H. Baur and D. Kassner, *Acta Crystallogr. Sect. B: Struct. Sci.*, 1992, **48**, 356.
97.   S. L. Mayo, B. D. Olafson and W. A. Goddard, *J. Phys. Chem.*, 1990, **94**, 8897.
98.   A. Irfan and J. Zhang, *Theor. Chem. Acc.*, 2009, **124**, 339.
99.   A. Irfan, R. Cui, J. Zhang and M. Nadeem, *Aust. J. Chem.*, 2010, **63**, 1283.